Terahertz Source Radiating to Open Space Based on the Superconducting Flux-Flow Oscillator: Development and Characterization

Nickolay V. Kinev, Kirill I. Rudakov, Lyudmila V. Filippenko, Andrey M. Baryshev, and Valery P. Koshelets

***Abstract*—We have elaborated, fabricated, and tested a terahertz source based on the Josephson flux-flow oscillator (FFO) integrated with a transmitting lens antenna. The oscillator was coupled to the on-chip double-slot antenna via microstrip lines, and the chip was mounted on the silicon lens providing the continuous terahertz emission output. The oscillator samples were made of superconductor–insulator–superconductor (SIS) trilayers based on Nb/AlN/NbN, with a gap voltage of about 3.6 mV. The output emission was studied using two independent techniques: a THz spectrometer based on the SIS receiver with a high spectral resolution (better than 0.1 MHz) and an Si bolometer. An operating range of the oscillator of 400–580 GHz and a ratio of detected signal to background signal at the receiver output of up to 55 dB are obtained. In addition, a design for the oscillator with an integrated harmonic mixer for FFO locking is developed and fabricated using Nb/AlO$_x$/Nb trilayers, which is better for FFO operation than Nb/AlN/NbN trilayers at some frequencies due to lower surface losses and hence better spectral properties. The pumping of the mixer by the FFO output power was measured and found to be sufficient for phase locking.**

***Index Terms*—Harmonic mixers (HM), Josephson effect, superconducting integrated circuits, terahertz oscillators, transmitting antennas.**

Manuscript received June 14, 2019; revised August 27, 2019 and September 10, 2019; accepted September 10, 2019. Date of publication September 13, 2019; date of current version November 4, 2019. This work was supported in part by the Russian Science Foundation under Project 17-79-20343, which funded numerical simulations, fabrication, and experimental study of the samples, in part by the Russian Science Foundation under Project 19-19-00618, which funded the development and optimization of the technology for fabrication of tunnel junctions with sub-μm dimensions, and technological maintenance, and in part by the Unique Science Unit (USU #352529), developed within the framework of the state task, which carried out the fabrication. *(Corresponding author: Nickolay V. Kinev.)*

N. V. Kinev, L. V. Filippenko, and V. P. Koshelets are with the Kotel'nikov Institute of Radio Engineering and Electronics of the Russian Academy of Sciences, Moscow 125009, Russia (e-mail: nickolay@hitech.cplire.ru; lyudmila@hitech.cplire.ru; valery@hitech.cplire.ru).

K. I. Rudakov is with the Kotel'nikov Institute of Radio Engineering and Electronics of the Russian Academy of Sciences, Moscow 125009, Russia, and also with the Kapteyn Astronomical Institute, University of Groningen, Groningen 9712 CP, The Netherlands (e-mail: k.rudakov@astro.rug.nl).

A. M. Baryshev is with the Kapteyn Astronomical Institute, University of Groningen, Groningen 9712 CP, The Netherlands (e-mail: andrey@astro.rug.nl).

Color versions of one or more of the figures in this article are available online at http://ieeexplore.ieee.org.

Digital Object Identifier 10.1109/TTHZ.2019.2941401

I. Introduction

A FLUX-FLOW oscillator (FFO) is a superconducting Josephson junction acting as a voltage-controlled oscillator based on the emission of the electromagnetic waves at collision of the unidirectional flow of magnetic vortices (Josephson fluxes) with the edge of the junction. Its frequency f is strictly determined by only the dc voltage $V_{\rm DC}$ across the junction, in accordance with the Josephson equation $hf = 2eV_{\rm DC}$. The FFO is circumstantially investigated in a set of interconnected papers by Nagatsuma *et al*. [1]–[4]. Since then, the oscillator has been modified considerably [5]–[7] and characterized with a high accuracy, using a harmonic mixer (HM) for downconversion of output emission to the range of 0.1–1 GHz and a phase-locking loop (PLL); the signal in this range can be measured directly using a spectrum analyzer with a high resolution. Modern properties of the FFO are as follows: an output frequency range of 300–700 GHz with continuous tuning, a linewidth in a free-running regime of about 0.5–15 MHz, depending on the operating regime, phase locking of emission power in a narrow peak with a width of about 40 kHz and a spectral ratio up to 95%, and output power sufficient for heterodyne receiving. This set of characteristics enabled successful implementation of the FFO as the local oscillator of a heterodyne receiver for the TELIS flight mission [8]–[9]. This receiver is based on a superconductor–insulator–superconductor (SIS) mixer and is known as a superconducting integrated receiver [10] (SIR), due to the integration of the FFO on a single chip with the SIS mixer.

Recently, we elaborated a novel concept for an FFO-based oscillator radiating to open space by integrating the FFO and a transmitting double-slot antenna on a single chip [11]–[12]. In the mentioned papers, we used a type of antenna that had previously been studied by Filipovic *et al.* as a receiving antenna coupled to a SIS mixer [13]. In this article, we have developed (see Section II) and tested (see Section III) a double-slot antenna with an alternative type of excitation and topology. This antenna is demonstrated to have a higher efficiency than the one used in our previous study (as discussed in Section III-C). This type of topology and excitation of the antenna was also previously used in [14] as a receiving antenna matched to a SIS detector at 500 GHz. In [12], we used the SIR for studying emission spectra in the range 497–700 GHz (available for the SIR operation), but it was not possible to study carefully the properties of the antenna over its whole bandwidth due to wider antenna's bandwidth than

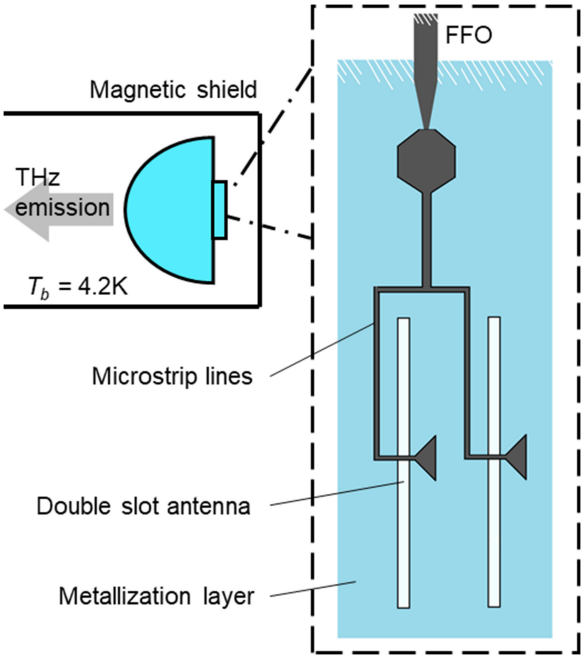

Fig. 1. Layout of the FFO-based terahertz source. On the right: the planar integrated structure containing the FFO, the slot antenna, and the microstrip transmission line containing an impedance transformer directly on the FFO output point. The length of the slots is 260 μm, the width is 4 μm, and the distance between the centers is 90 μm. On the left: the chip with the integrated structure mounted on the silicon lens and placed inside a magnetic shield in a cryogenic system with a temperature of 4.2 K.

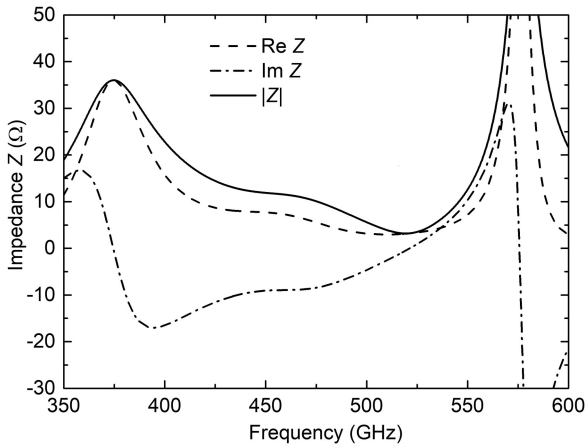

Fig. 2. Numerically simulated impedance Z of the transmitting double-slot antenna. The real part, the imaginary part, and the absolute value of Z are presented.

that of the SIR. In this article, we used a cooled Si bolometer with infrared (IR) filters as a microwave detector for studying the transmission properties of the antenna over the whole operating region (see Section III-B). In addition, we used the same technique as in [12], based on the SIR, to compare the emission power and hence the efficiency of the two types of topology and excitation of the double-slot antenna (see Section III-C).

The applicability of the oscillator is determined by the spectral properties of the emission. It is known [5]–[10] that the FFO should be phase locked for practical applications (e.g., the ground-based or the flight space missions), and therefore we made a first effort to design an HM coupled to the FFO integrated with the same double-slot antenna (see Section IV). The pumping of the HM by the FFO emission was observed directly measuring the current–voltage curves (IVCs) and is found to be sufficient for locking of the oscillator by means of the PLL.

II. Design and Simulations

A long tunnel junction with a length of 400 μm was used to operate as the FFO; this length is much greater than the Josephson penetration depth of a few μm, with a small output impedance of only fractions of an ohm at the frequency of operation. For providing the THz emission to open space, the FFO output was coupled via a microstrip line to a double-slot antenna. The concept of the FFO-based emitter is presented in Fig. 1. Pattern of antenna, as well as the base electrodes of the FFO and the microstrip line, all are made from Nb in the same metallization layer. Both the substrate of the chip and the extended semielliptical lens are made of Si, with a dielectric constant of $\varepsilon = 11.7$. The extension length of the lens (0.994 mm) was specially designed, taking into account the thickness of the substrate (0.535 mm), to ensure that the center of the antenna is located at the far focus of the lens. The center of the antenna is located at the very center of the chip, and the chip is mounted at the very center of the lens using a microscope with the movable table with the accuracy of 1 μm. The chip is stuck to the lens with a cyanoacrylate glue.

The FFO tunnel structure was fabricated from Nb/AlN/NbN or Nb/AlO_x/Nb trilayers with a current density of about $7 \div 8$ kA/cm^2, corresponding to a normal-state resistance–area product $R_n \times A = 25 \div 30\,\Omega \cdot \mu\text{m}^2$. The antenna was fabricated from Nb film, and the microstrip lines were fabricated from Nb electrodes with a SiO_2 insulation layer, with a dielectric constant of $\varepsilon = 4.2$ for thin films.

For design purposes and for numerical simulations of the properties of the integrated structure at THz frequencies, specialized software CST Studio for three-dimensional microwave calculations was used. The London penetration depth for Nb films of 85 nm is used for taking into account the superconducting state of the microstrips and the antenna. The output impedance of the FFO is taken to be independent on frequency and swept in a range between 0.5 and 1.5 Ω. As a result, the layout shown in Fig. 1 was designed, and the frequency dependencies of both the impedance of the antenna and the emission to open space were calculated. The impedance at the point of connection to the impedance transformer is shown in Fig. 2. The bandwidth of the antenna, according to the calculated power radiated to open space, varies from 380–520 GHz to 400–500 GHz depending on the output impedance of the FFO. A detailed picture is shown in Section III-B, together with experimental results for comparison. The operating bandwidth of 120–140 GHz obtained for this design is about 0.3 of the central frequency, which is a typical and reliable result for double-dipole and double-slot types of antennas.

III. Measurements

A. Fabrication

A few batches of the samples based on Nb/AlN/NbN tunnel junctions [15]–[16] with dimensions 4 mm × 4 mm were fabricated on the Si substrate (thickness 0.535 mm). To prevent etching of the substrate material in the process of plasma etching during the junction definition process, a buffer layer of Al_2O_3 (thickness of about 100 nm) was deposited by RF magnetron sputtering. The next step is the deposition of a trilayer Nb/AlN/NbN structure; it was carried out using a dc magnetron sputtering in a single vacuum run. First, a layer of lower Nb with a thickness of 200 nm is deposited, then a layer of Al with a thickness of 7 nm. The AlN tunnel barrier was grown an immediately after Al deposition by using RF magnetron discharge [15]. Then the 100-nm NbN layer was deposited by dc magnetron sputtering in a mixture of Ar and N_2. The geometry of the base electrode was formed by lift-OFF. The SIS junctions are formed by plasma-chemical etching in CF_4 by removing the top NbN layer of the trilayer structure according to the mask from the photoresist determining the junction geometry. The barrier layer AlN acts as a stop layer preventing further etching of the structure. After plasma-chemical etching, anodizing is performed up to 10 V using the same photoresist mask; then an insulating SiO_2 layer, typical thickness of which is 400 nm, is deposited by RF magnetron sputtering. Opening of contacts to the junctions is carried out by lift-OFF. The top electrode is also formed by lift-OFF from the sputtered Nb layer of 400–450 nm thick. The gold contact pads to the base and top electrodes are formed in a similar way. The dimensions of the FFO are 16 μm × 400 μm that have been previously used in [8], [9], and [12].

A normal-state resistance–area product $R_n \times A$ of $\sim 19\,\Omega \cdot \mu\text{m}^2$ is obtained by dc testing of the fabricated SIS trilayer. This differs from the expected value of 25 $\Omega \cdot \mu\text{m}^2$ used for numerical simulations. The gap voltage V_g is about 3.5 mV, and the subgap resistance to the normal-state resistance ratio R_j/R_n is about 30, which is a good result for the Nb/NbN technique. The typical IVC of the test SIS junction is shown in Fig. 3.

B. Operating Range

For the study of the emission to open space and the frequency properties of the transmitting antenna, a wideband microwave direct detector based on the Si bolometer was used. The scheme of the experimental setup and the photograph are shown in Fig. 4. Two 4.2 K liquid helium cryostats were used simultaneously: cryostat #1 for cooling down the FFO microcircuit mounted on the lens and cryostat #2 for cooling down the bolometer located opposite the oscillator. IR filters transparent in the THz range are used in both cryostats. The filters, made of Gore-Tex, were installed inside cryostat #1 at the 77 K and 4.2 K stages, to avoid heating the FFO via radiation from outer space. A quartz filter was mounted in cryostat #2 at the input of the bolometer, to minimize the strong background signal in the IR range and to provide the distinction of a weaker THz signal. The bolometer output signal (response) was measured using a lock-in amplifier,

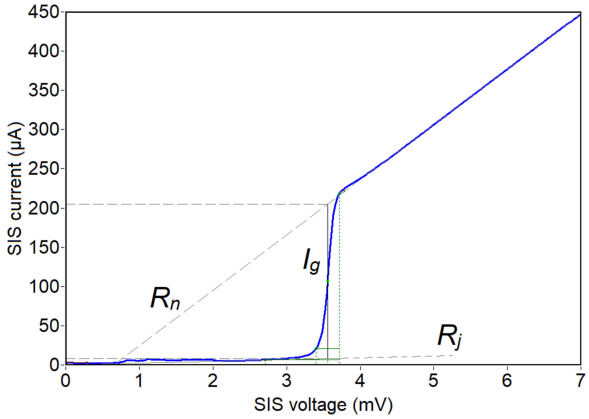

Fig. 3. IVC of Nb/AlN/NbN-based test SIS junction with an area of $\sim$1.4 μm^2 on the fabricated batch. The specific parameters are as follows: normal-state resistance $R_n = 14.2\,\Omega$, ratio $R_j/R_n = 30.8$, $V_g = 3.56$ mV, and current jump at the gap voltage $I_g = 197\,\mu$A. Some supplementary dashed curves are shown for defining the parameters.

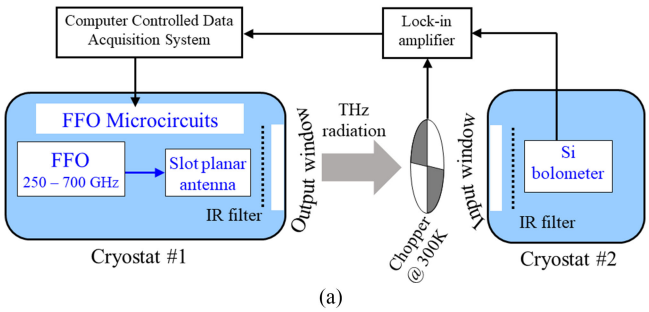

(a)

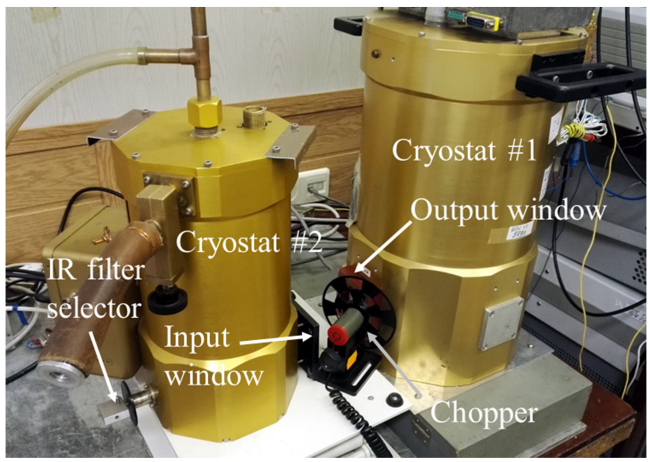

(b)

Fig. 4. (a) Block diagram of the experimental setup for studying the radiation of the FFO-based source radiating to open space, using a cooled Si bolometer. (b) Photo of the main parts of the experimental setup, not including measuring instruments.

so that the emission was modulated by an optical chopper with a frequency of about 170 Hz.

The FFO is fully controlled by applying two currents: one for dc biasing the Josephson junction I_B and the second one for supplying the local magnetic field using a control line I_{CL}. The dc voltage V_B was measured using the additional terminals, so a four-point biasing current-control scheme was implemented

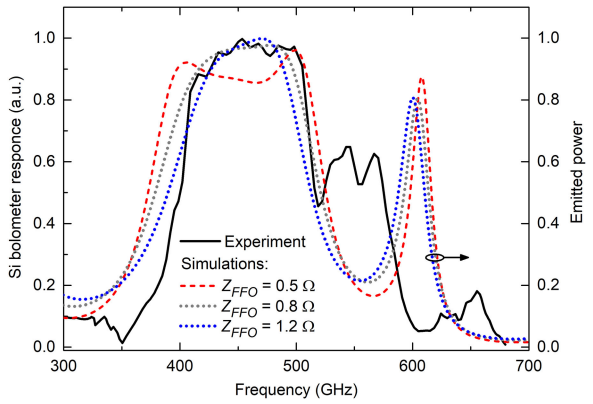

Fig. 5. FFO emission to open space detected by the Si bolometer (solid curve, related to the left axis) and numerical simulations of emitted power normalized to the total output power (dashed and dotted curves, related to the right axis) obtained using different FFO output impedance Z_{FFO}.

for better accuracy. The contact pads of the chip were bonded to the bias plate using Al wires with a diameter of 25 μm. It is interesting to note that the emission frequency is precisely defined by the FFO bias voltage V_B; therefore, there is no need to use any other techniques for frequency determination. The accuracy of frequency determination in this setup of $\sim$0.5 GHz is equivalent to the accuracy of voltage measurement, which is about 1 μV with using a battery current supply.

The emission of the FFO-based source was detected by the Si bolometer over the full range of the FFO operation. The complete frequency range was studied via slow sweeping of the FFO voltage with a small step size of $\sim$1–2 μV (corresponding to a frequency step of $\sim$0.5–1 GHz). The voltage was swept by sweeping the current I_{CL} supplying the magnetic field with a step size of 0.05 mA in the range from 30 up to 90 mA. This sweeping was carried out over the wide range of the bias current I_B from 17 up to 35 mA with a step size of 1 mA. The experimental results are presented in Fig. 5 and compared with numerical simulations. A reasonable agreement between experimental data and numerical simulations is obtained for the main peak. The exact values of some parameters are unknown, such as a London penetration depth for Nb films, a dielectric constant and a thickness of SiO_2 fabricated films, as well as the FFO output impedance Z_{FFO}. It was found that the numerical results are most sensitive to changing of Z_{FFO}, and the results for values of 0.5, 0.8, and 1.2 Ω are shown in Fig. 5. It is difficult to say if the second double peak in the experiment having a center frequency of $\sim$550 GHz and a half intensity of the main peak is related to the second narrow peak in simulations with a frequency of $\sim$600 GHz or not related. It should be also noted that some effects leading to decrease of the emitting power were not taken into account in simulations. One of those is damping of the signal in the experiment caused by increased surface losses in Nb lines at frequencies higher than 650 GHz, in accordance to the Mattis–Bardeen theory. Another reason for damping at higher frequencies is self-pumping effect in a long Josephson junction at the voltage above $V_g/3$ [17], [18].

To summarize, an operating range of 400–580 GHz, at the level of 0.5 of the maximum emitted power of the developed "FFO & lens antenna" integrated structure, is obtained experimentally and corresponds adequately to the simulations.

C. Spectral Properties

The spectral properties of the emission are studied with a resolution better than 0.1 MHz, utilizing a spectrometer based on the superconducting integrated receiver. A scheme for the experimental setup is shown in Fig. 6. As for the setup with the Si bolometer, two liquid helium cryostats were used: cryostat #1 for cooling down the FFO microcircuit mounted on the lens and cryostat #2 for the SIR microcircuits. The SIR operation (the whole right part in Fig. 6) is described in detail elsewhere [10], [19], [20]. Two FFOs were used simultaneously in the experimental setup: one (FFO #1) is the core of the emitter under study and the other (FFO #2) is used as the local oscillator of the SIR. The spectral shape of the emission line was registered by the spectrum analyzer in the intermediate frequency (IF) range of 4–8 GHz, and the SIS output signal was gained by the IF amplifiers. The amplification chain consists of both the cryogenic amplifier based on a high electron mobility transistor (HEMT) with a gain of about 30 dB, and the room temperature amplifier with a gain of about 60 dB, so total gain is about 90 dB. Since there was no ability to lock the radiating signal of FFO #1, the shape of the emission line could not be measured accurately by averaging large number due to frequency fluctuations.

The FFO emission lines are registered over the wide range of operation, from 440 up to 700 GHz, available for the SIR. The recorded spectra of the free-running emission at various frequencies with steps multiple of 20 GHz are presented in Fig. 7. The averaging number $N = 3$ was used to record the shape and the amplitude of the lines. All the lines were recorded close to the center of the IF range, which is at 6 GHz, but in Fig. 7, the curves are slightly shifted in frequency, to distinguish them from each other for clarity.

There are a few points to discuss regarding the results. First of all, the ratio of detected signal to IF background signal at the receiver output is about 55 dB for the strongest emission lines (see 500 and 520 GHz in Fig. 7) and up to 30 dB for the weak emission lines at the upper border of the operating range (see 640 and 700 GHz). This is a good result, demonstrating the applicability of the oscillator to different tasks. Furthermore, this signal ratio is much better than the results obtained earlier in [12] for another type of excitation and topology of slot antenna, where a ratio of about 25–30 dB was obtained for the strongest lines. Despite the fact that there is still no HM for phase locking in the current antenna design, this topology of antenna seems to be more promising than the one studied previously. Finally, there seems to be some contradiction between the results in Figs. 5 and 7, since there is almost the same emission power in the range 420–500 GHz according to Fig. 5, but the difference in power of the peaks at 440 and 500 GHz is about 20 dB according to Fig. 7. In fact, there is no disagreement due to several reasons. The main reason is different conversion losses of SIS mixer at different frequencies leading to completely different sensitivity of the receiver, whereas the sensitivity of the Si bolometer is almost the same over the complete operating range of the FFO. The mixer is

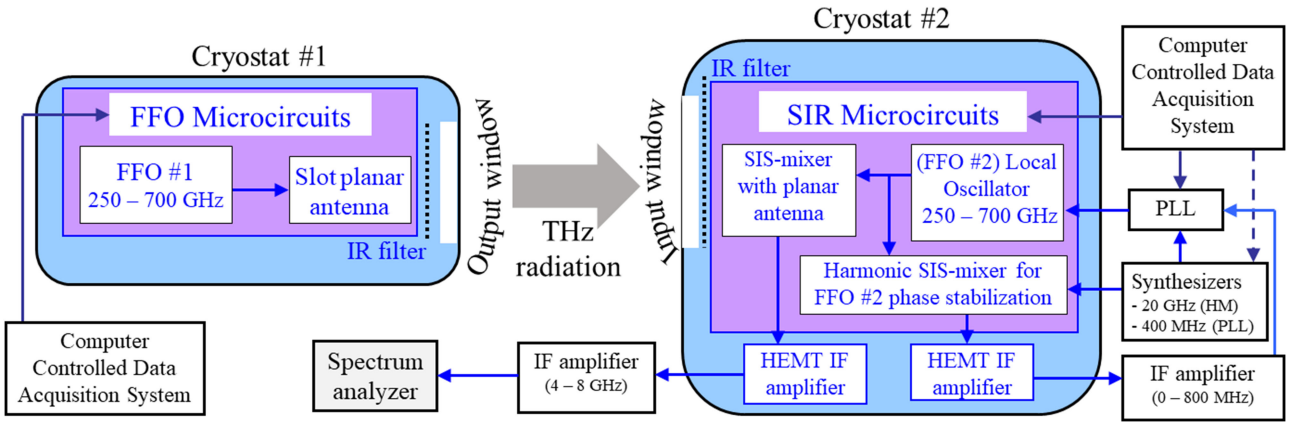

Fig. 6. Block diagram of the experimental setup for studying the FFO emission to open space using a THz spectrometer, based on the superconducting integrated receiver.

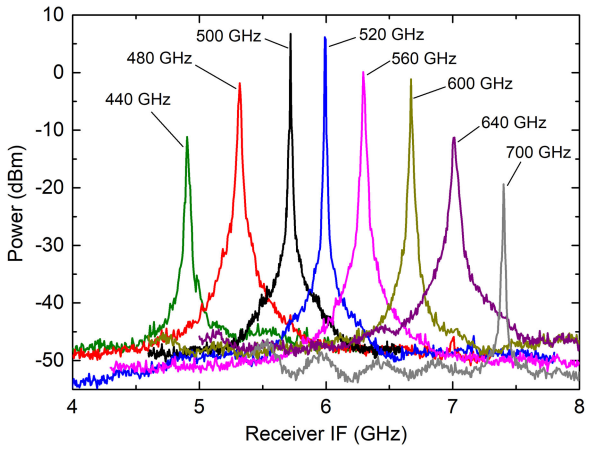

Fig. 7. Power spectra of the FFO at some selected frequencies, measured using the spectrometer based on the SIR. The frequency of emission is indicated for each curve. The resolution bandwidth of the spectrum analyzer is 1 MHz.

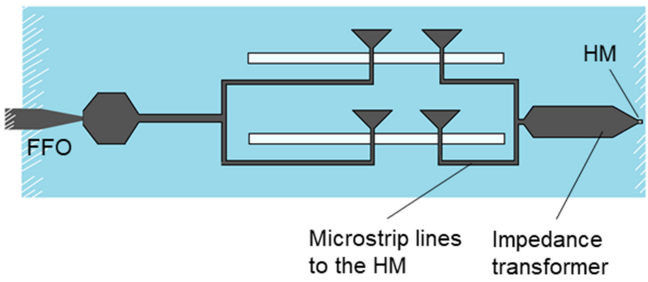

Fig. 8. Layout of the FFO-based planar integrated structure containing the FFO, the slot antenna, the HM, and the microstrip lines between the elements (design #1). An impedance transformer is used just in front of the HM. The layout is different from that presented in Fig. 1 due to the embedding the HM, and all the other parts are the same.

designed so that its capacitance is tuned the best for the frequency range 500–600 GHz; below and upper of this range a conversion efficiency decreases considerably. The best noise temperature of the SIR is at ~500–510 GHz (about 130 K) and ~600–605 GHz (about 200 K), and it increases below 500 down to 440 GHz [8]. Besides that, the beam patterns of both the oscillator and the receiver are slightly different at different frequencies, and the best position of cryostats relative to each other was found at 500 GHz. A difference of a few dB in detecting signal at other frequencies can occur due to optical coupling. Therefore, the power detected by the SIR at 440 and 480 GHz is less than that detected at 500 and 520 GHz.

IV. HM for FFO Phase Locking

For practical applications as a local osillator, the FFO should be phase locked. For this purpose, an HM based on the SIS junction and the PLL are commonly used [5]–[12]. A small part of the FFO power should be branched to the HM by the matching transmission line. The pumping of the HM at ~5–20% of the current jump at the gap voltage is sufficient for proper mixing of the FFO signal and a harmonic of ~20 GHz from the reference synthesizer. The typical setup for the FFO phase locking is shown in Fig. 6 for FFO #2 as a part of the SIR.

We have attempted to embed the HM into the developed FFO-based integrated structure without changing the geometry of the slot antenna, and we performed preliminary testing for the pumping current. The principle of embedding and the layout of the integrated structure with the HM are shown in Fig. 8 for design #1. Design #2 differs in the points of connection of the microstrips at the slots to the HM. The HM, with a SIS junction area ~1.4 μm^2, is fabricated in the same technological cycle as the FFO.

A batch of samples based on Nb/AlO$_x$/Nb tunnel trilayers was fabricated according to developed designs #1 and #2 containing the FFO, the HM and the transmitting antenna. For this batch, Nb/AlO$_x$/Nb trilayer instead of Nb/AlN/NbN is used due to lower surface losses at some frequencies and hence the lower spectral linewidth of the emission, which is proportional to squared differential resistance of the SIS junction [5], [7].

According to dc testing, the parameters of the tunnel structures are as follows: the normal-state resistance–area product $R_n \times A$ is 32 $\Omega \cdot \mu$m^2, corresponding to a current density of ~6.6 kA/cm^2, the gap voltage is 2.68 mV, and the subgap resistance to the normal-state resistance ratio R_j/R_n is about 25, which is a proper result for the all-Nb technique. The area of the HM on the chip with design #1 is 1.69 μm^2, and with design #2 is

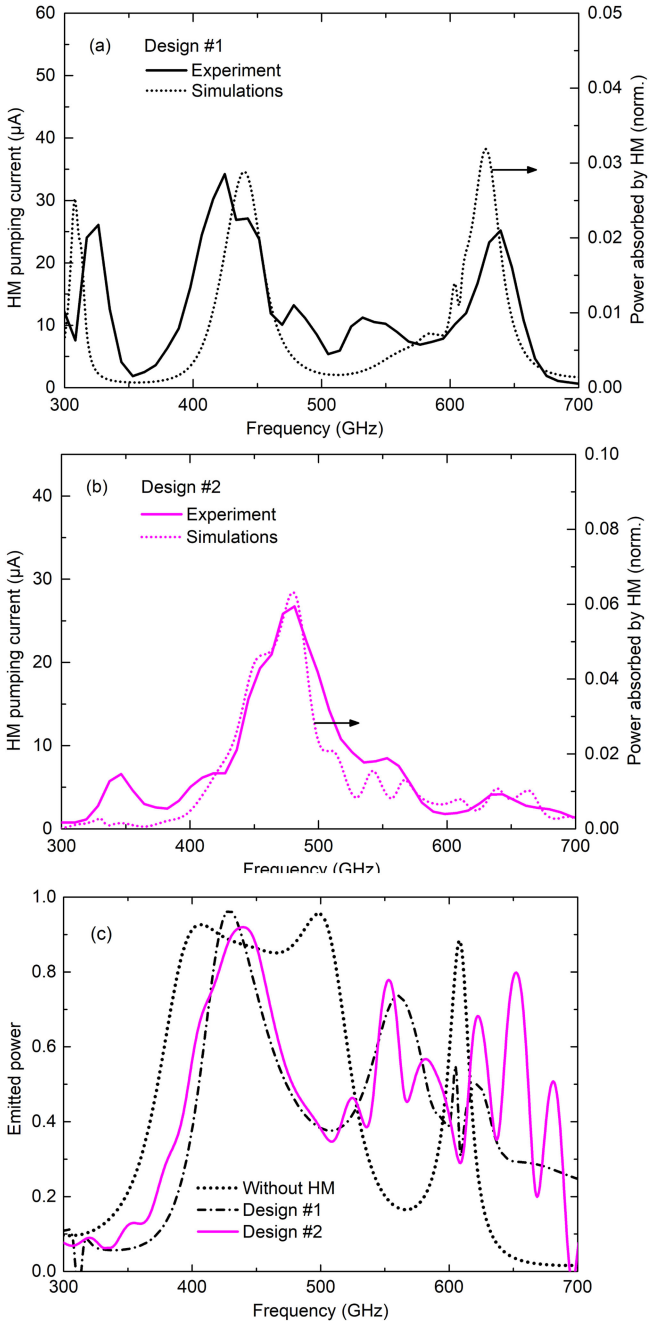

Fig. 9. Experimental results of HM pumping by the FFO power (solid curves, relating to the left axis) and numerical simulations of the FFO power absorbed by the HM (dotted curves, relating to the right axis) for the sample of (a) design #1 and (b) design #2. The power absorbed by the HM in numerical simulations is normalized to the total FFO output power. (c) Emitted power of the FFO-based source to open space normalized to the total output power for design #1 (dash–dotted curve) and design #2 (solid curve) according to numerical simulations. Emitted power for the design without HM (dotted curve), as discussed in Sections II and III, is also shown for comparison, and is the same as the dashed curve in Fig. 5.

1.4 μm^2; these parameters were used in the numerical simulations for the corresponding design. The pumping of the HM was measured as the current quasi-particle step on the IVC induced by the FFO power, utilizing the usual dipstick dc testing in liquid helium. The results for HM pumping observed experimentally and in the numerical simulations, are shown in Fig. 9(a) and (b), and those for numerical simulations of the emission to open space are shown in Fig. 9(c), for both designs #1 and #2. It is important to note that the results of the numerical simulations are rather sensitive to the area of the HM junction, and therefore the simulations have been carried out according to the values of already-fabricated samples (1.69 μm^2 and 1.4 μm^2 for designs #1 and #2 respectively). Otherwise, it would be less correct to compare the experimental and calculated data in the case of deviations in the HM area due to technological error. There are some points to discuss regarding the results in Fig. 9. First, the relative width of the peaks in the experiment and that in the simulations, as well as frequencies of the peaks, are in reasonable agreement. Second, it can be seen that design #1 is more wideband than design #2, in the sense of the FFO phase-locking capability. The current jump at the gap voltage is 120 μA for the HM in design #1 and 98 μA for the HM in design #2. Normally, an HM pumping level of 5–10% of the current jump is sufficient for proper PLL operation, which is equal to 6–12 μA for the sample of design #1 and 5–10 μA for the sample of design #2. Hence, the bandwidth for design #1, according to dc testing, is expected to be 400–650 GHz (there could be some shortage of pumping power at frequencies close to 500 GHz), and for design #2 it is expected to be 430–570 GHz. Finally, the embedding of the HM in both designs #1 and #2 substantially narrows the frequency range of emission to open space at the level above 0.7, in comparison with the design without HM [see dotted and solid curves in Fig. 9(c)]. We represent a few trials only, and the layout still requires substantial optimization for more wideband operation of such a complex integrated structure. Nevertheless, this concept of connection of the HM to the "FFO & antenna" structure seems to be promising and improvements appear to be possible. According to numerical simulations, the range of the emission to open space at the level of 0.4 of the total FFO power is from 400 GHz up to about 600 GHz for both designs #1 and #2. Therefore, such THz source based on the phase locked FFO can be successfully used as a heterodyne for THz receivers in the ground-based or the flight mission, and can be mounted on the same cold plate as THz mixer based on SIS junction or hot electron bolometer. Another possible application is a multifunctional laboratory phase locked THz source with wideband tuning. The oscillator can be used as an active source for THz spectroscopy, THz microscopy, studying the properties of material at THz frequencies at low temperatures.

V. Conclusion

The terahertz FFO is a promising solution for THz applications, due to an ultrawide operating range (up to 100% of the central frequency) for a single sample. We proposed, elaborated, and experimentally studied the concept of the FFO-based emitter to open space, utilizing a transmitting double-slot antenna and an extended semielliptical lens. In the first stage, we numerically simulated the integrated structure for an output emission bandwidth of 380–520 GHz. Then, we fabricated samples based on Nb/AlN/NbN Josephson junctions and studied the THz emission

to open space, using two different techniques. The operating region was determined using a cooled Si bolometer, and a range of 400–580 GHz is obtained, which is wider than that obtained in numerical simulations. The spectral properties of the output emission were studied using a superconducting SIS receiver with a phase-locked local oscillator. A spectral line with a ratio of detected signal to IF background signal at the receiver output up to 55 dB is obtained in the range 440–700 GHz, available for receiver operation. In addition, we performed preliminary elaboration and testing of designs of the FFO-based emitter containing an HM for phase locking of the FFO. The samples were fabricated from Nb/AlO_x/Nb trilayers. The pumping of the HM in the range 400–650 GHz is obtained and is expected to be sufficient for phase locking.

The design of the integrated structure containing the oscillator, the antenna and the HM, can be improved by increasing the operating bandwidth defined by matching of the elements. Also, the development of designs for specific frequencies required for particular tasks can be made. The oscillator based on the principle discussed in this article can be elaborated for any operating frequency band up to 700 GHz if Nb-based transmission lines are used. For increasing the upper limit of the frequency range up to 1 THz, Al/NbTiN-based transmission lines with much lower surface losses should be used.

References

[1] T. Nagatsuma, K. Enpuku, F. Irie, and K. Yoshida, "Flux-flow type Josephson oscillator for millimeter and submillimeter wave region," *J. Appl. Phys.*, vol. 54, no. 6, pp. 3302–3309, Jun. 1983, doi: 10.1063/1.332443.

[2] T. Nagatsuma, K. Enpuku, K. Yoshida, and F. Irie, "Flux-flow-type Josephson oscillator for millimeter and submillimeter wave region. II. Modeling," *J. Appl. Phys.*, vol. 56, no. 11, pp. 3284–3293, Dec. 1984, doi: 10.1063/1.333849.

[3] T. Nagatsuma, K. Enpuku, K. Sueoka, K. Yoshida, and F. Irie, "Flux-flow-type Josephson oscillator for millimeter and submillimeter wave region. III. Oscillation stability," *J. Appl. Phys.*, vol. 58, no. 1, pp. 441–449, Jul. 1985, doi: 10.1063/1.335643.

[4] J. Qin, K. Enpuku, and K. Yoshida, "Flux-flow-type Josephson oscillator for millimeter and submillimeter wave region. IV. Thin-film coupling," *J. Appl. Phys.*, vol. 63, no. 4, pp. 1130–1135, Feb. 1988, doi: 10.1063/1.340019.

[5] V. P. Koshelets *et al.*, "Phase locked 270–440 GHz local oscillator based on flux flow in long Josephson tunnel junctions," *Rev. Sci. Instrum.*, vol. 71, no. 1, pp. 289–293, Jan. 2000, doi: 10.1063/1.1150195.

[6] V. P. Koshelets *et al.*, "Towards a phase-locked superconducting integrated receiver: Prospects and limitations," *Physica C*, vol. 367, nos. 1–4, pp. 249–255, Feb. 2002, doi: 10.1016/S0921-4534(01)01046-2.

[7] V. P. Koshelets *et al.*, "Optimization of the phase-locked flux-flow oscillator for the submm integrated receiver," *IEEE Trans. Appl. Supercond.*, vol. 15, no. 2, pp. 964–967, Jun. 2005, doi: 10.1109/TASC.2005.850140.

[8] G. Lange *et al.*, "Development and characterization of the superconducting integrated receiver channel of the TELIS atmospheric sounder," *Supercond. Sci. Technol.*, vol. 23, no. 4, pp. 045016-1–045016-8, Mar. 2010, doi: 10.1088/0953-2048/23/4/045016.

[9] V. P. Koshelets *et al.*, "Superconducting integrated terahertz spectrometers," *IEEE Trans. Terahertz Sci. Technol.*, vol. 5, no. 4, pp. 687–694, Jun. 2015, doi: 10.1109/TTHZ.2015.2443500.

[10] V. P. Koshelets and S. V. Shitov, "Integrated superconducting receivers," *Supercond. Sci. Technol.*, vol. 13, no. 5, pp. R53–R69, 2000, doi: 10.1088/0953-2048/13/5/201.

[11] N. V. Kinev, K. I. Rudakov, L. V. Filippenko, A. M. Baryshev, and V. P. Koshelets, "Wideband Josephson THz flux-flow oscillator integrated with the slot lens antenna and the harmonic mixer," in *Proc. EPJ Web Conf.*, vol. 195, Nov. 2018, pp. 02003-1–02003-2, doi: 10.1051/epjconf/201819502003.

[12] N. V. Kinev, K. I. Rudakov, L. V. Filippenko, A. M. Baryshev, and V. P. Koshelets, "Flux-flow Josephson oscillator as the broadband tunable terahertz source to open space," *J. Appl. Phys.*, vol. 125, no. 15, pp. 151603-1–151603-7, Mar. 2019, doi: 10.1063/1.5070143.

[13] D. F. Filipovic, S. S. Gearhart, and G. M. Rebeiz, "Double-slot antennas on extended hemispherical and elliptical silicon dielectric lenses," *IEEE Trans. Microw. Theory Tech.*, vol. 41, no. 10, pp. 1738–1749, Oct. 1993, doi: 10.1109/22.247919.

[14] J. Zmuidzinas and H. G. LeDuc, "Quasi-optical slot antenna SIS mixers," *IEEE Trans. Microw. Theory Techn.*, vol. 40, no. 9, pp. 1797–1804, Sep. 1992, doi: 10.1109/22.156607.

[15] P. N. Dmitriev *et al.*, "High quality Nb-based integrated circuits for high frequency and digital applications," *IEEE Trans. Appl. Supercond.*, vol. 13, no. 2, pp. 107–110, Jun. 2003, doi: 10.1109/TASC.2003.813657.

[16] A. Khudchenko *et al.*, "High-gap Nb-AlN-NbN SIS junctions for frequency band 790–950 GHz," *IEEE Trans. Terahertz Sci. Technol.*, vol. 6, no. 1, pp. 127–132, Dec. 2016, doi: 10.1109/TTHZ.2015.2504783.

[17] A. L. Pankratov, A. S. Sobolev, V. P. Koshelets, and J. Mygind, "Influence of surface losses and the self-pumping effect on current-voltage characteristics of a long Josephson junction," *Phys. Rev. B*, vol. 75, no. 18, pp. 184516-1–184516-5, May 2007, doi: 10.1103/PhysRevB.75.184516.

[18] D. R. Gulevich, V. P. Koshelets, and F. V. Kusmartsev, "Josephson flux-flow oscillator: The microscopic tunneling approach," *Phys. Rev. B*, vol. 96, no. 2, pp. 024515-1–024515-1, Jul. 2017, doi: 10.1103/PhysRevB.96.024515.

[19] O. Kiselev *et al.*, "Balloon-borne superconducting integrated receiver for atmospheric research," *IEEE Trans. Appl. Supercond.*, vol. 21, no. 3, pp. 612–615, Jun. 2011, doi: 10.1109/TASC.2010.2091712.

[20] V. P. Koshelets *et al.*, "Integrated submmwave receiver: Development and applications," in *Fundamentals of Superconducting Nanoelectronics*. Berlin, Germany: Springer, 2011, ch. 10, pp. 263–296, doi: 10.1007/978-3-642-20158-5_10.

Nickolay V. Kinev received the B.S. degree in applied mathematics and physics and the M.S. degree in solid-state electronics and radio physics from the Moscow Institute of Physics and Technology, Moscow, Russia, in 2007 and 2009, respectively, and the Ph.D. degree from the Kotel'nikov Institute of Radio Engineering and Electronics of the Russian Academy of Sciences, Moscow, Russia, in 2013. His dissertation was on the study and development of terahertz oscillators and receivers using superconducting devices.

He is currently a Senior Researcher with the Kotel'nikov Institute of Radio Engineering and Electronics of the Russian Academy of Sciences, Moscow, Russia. His research interests include superconducting receivers and oscillators for terahertz technologies and space applications.

Dr. Kinev was a recipient of the Government of Moscow Young Scientist Award in 2018 for the contribution to the study of superconducting terahertz sources.

Kirill I. Rudakov received the B.S. and M.S. degrees in applied physics and mathematics from the Moscow Institute of Physics and Technology, Moscow, Russia, in 2013 and 2015, respectively. He is currently working toward the Ph.D. degree in the Kapteyn Astronomical Institute, University of Groningen, Groningen, The Netherlands.

Since 2012, he has been with the Kotel'nikov Institute of Radio Engineering and Electronics of the Russian Academy of Sciences, Moscow, Russia. After internships as a Research Student in the ALPHA experiment at CERN in 2013 and as a Guest Scientist in the CHAMP+ experiment at a SRON in 2014, he started a Ph.D. research with the Kapteyn Astronomical Institute, University of Groningen, Groningen, The Netherlands, in 2016. His Ph.D. research is devoted to the modeling and development of elements of the array SIS receivers in terahertz range. His research interests include heterodyne waveguide SIS-based receivers and high-frequency simulations of superconducting circuits, and measurements of them.

Lyudmila V. Filippenko received the M.S. degree from Saratov State University, Saratov, Russia, in 1986, and the Ph.D. degree from the Kotel'nikov Institute of Radio Engineering and Electronics of the Russian Academy of Sciences, Moscow, Russia, in 2009. Her Ph.D. dissertation was on the development of integrated superconducting receiving circuits based on high-quality tunnel junctions.

She is currently a Senior Researcher with the Kotel'nikov Institute of Radio Engineering and Electronics of the Russian Academy of Sciences, Moscow, Russia. Her research interests include development and fabrication of superconducting devices.

Andrey M. Baryshev received the M.S. degree (*summa cum laude*) in physical quantum electronics from the Moscow Institute of Physics and Technology, Moscow, Russia, in 1993, and the Ph.D. degree from the Technical University of Delft, Delft, The Netherlands, in 2005. His dissertation was on the study and development of SIS terahertz mixer integrated with a superconducting flux-flow oscillator.

He is currently a Senior Instrument Scientist. Since 1998, he has been with the SRON Low Energy Astrophysics Division and the Kapteyn Astronomical Institute, University of Groningen, Groningen, The Netherlands. Since 2000, he has been involved in a joint effort to develop an SIS receiver (600–720 GHz) for the Atacama Large Millimeter Array. In 2013, he became an Associate Professor of astronomical instrumentation for the Far-Infrared with Kapteyn Astronomical Institute, University of Groningen. His research interests include heterodyne and direct detectors for large focal plane arrays at THz frequencies and on quasi-optical system design and experimental verification.

Dr. Baryshev was the recipient of an NWO-VENI grant in 2008 for research on heterodyne focal plane array technology, and an EU commission Starting Researcher Grant for work on direct detector focal plane arrays, in 2009.

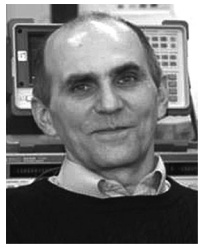

Valery P. Koshelets received the M.S. degree in physics from Lomonosov Moscow State University, Moscow, Russia, in 1973, and the Ph.D. degree in radio physics and Doctor of Sciences (Habilitation) degree in physical electronics from the Kotel'nikov Institute of Radio Engineering and Electronics of the Russian Academy of Sciences, Moscow, in 1978 and 1990, respectively.

Since 1973, he has been with the Kotel'nikov Institute of Radio Engineering and Electronics of the Russian Academy of Sciences, Moscow, Russia, where he is currently the head of the Laboratory of Superconducting Devices for Signal Detection and Processing.